FULL PAPER

Oxalate-Based 3D Chiral Magnets: The Series [Z^{II}(bpy)$_3$][ClO$_4$][M^{II}Fe^{III}(ox)$_3$] (Z^{II} = Fe, Ru; M^{II} = Mn, Fe; bpy = 2,2′-Bipyridine; ox = Oxalate Dianion)

Eugenio Coronado,*[a] José R. Galán-Mascarós,*[a] Carlos J. Gómez-García,[a] Eugenia Martínez-Ferrero,[a] Manuel Almeida,[b] and João C. Waerenborgh[b]

The synthesis, structure, and physical properties of the oxalate-based molecular magnets with the formula [Z^{II}(bpy)$_3$][ClO$_4$][M^{II}Fe^{III}(ox)$_3$] (Z^{II} = Fe, Ru; M^{II} = Mn, Fe; bpy = 2,2′-bipyridine; ox = oxalate dianion) are presented here. All compounds are isostructural and crystallize in the chiral cubic space group $P4_132$, and contain three-dimensional dimetallic networks formed by alternating M^{II} and M^{III} ions that are connected by oxalate anions. These compounds exhibit strong antiferromagnetic interactions that give rise to magnetic ordering as ferrimagnets or weak ferromagnets, with critical temperatures of up to 20 K, which is twice as high as those found for the isostructural magnets based on Cr^{III}, as determined by magnetic measurements and Mössbauer spectroscopy.

(© Wiley-VCH Verlag GmbH & Co. KGaA, 69451 Weinheim, Germany, 2005)

Introduction

Coordination chemistry has yielded many examples of molecule-based magnets. The nature of the ligands, responsible for promoting strong enough magnetic exchange, will be key for the physical properties found in these novel compounds. Most of these magnets are based on coordination polymers with metal centers that are connected by short ligands with a π-extended system such as cyanide,[1] dicyanamide[2–4] oxalate[5–7] and some other organic ligands.[8]

Polynuclear complexes from the oxalato ligand have been shown to be very versatile for the construction of magnetic materials, with one of the key reasons being the synthetic control over the lattice dimensionality. This has been demonstrated with the controlled obtention of dimers,[9] trimers,[10] 1D chains,[11] and extended 2D[5,6] and 3D lattices[12,13] from essentially the same building blocks. Interestingly, some of these coordination polymers are anions that form salts with a variety of molecular cations.

Bulky organic monocations promote the synthesis of compounds with the formula [A][M^{II}M^{III}(ox)$_3$] (A = NR$_4^+$, PPh$_4^+$; M^{II} = Mn, Fe, Co, Ni, Cu; M^{III} = Cr, Fe, Ru, Rh),[5,6,14–16] formed by two-dimensional oxalate bridged dimetallic networks. The sign of the magnetic interaction is determined by the nature of the metals – Cr^{III} and Ru^{III} promote ferromagnetic interactions, while Fe^{III} promotes antiferromagnetic interactions. These materials behave as ferromagnets with critical temperatures of up to 15 K, and as ferri- or weak ferromagnets with critical temperatures of up to 44 K. The combination of different trivalent metals in the 2D lattice has given rise to materials with tunable magnetic properties, and large hysteresis loops with coercive fields of over 2 T.[17] On the other hand, insertion of electroactive organometallic or organic molecules in these 2D systems has yielded magnetic multilayers,[18] ferromagnetic metals,[19,20] or photochromic magnets.[21]

Chiral octahedral complexes of the type [Z(bpy)$_3$]$^{2+}$ (bpy = 2,2′-bipyridine) and analogs favor the formation of the series [Z^{II}(bpy)$_3$][ClO$_4$][M^{II}M^{III}(ox)$_3$] (Z^{II} = Ru, Fe, Co, Ni; M^{II} = Mn, Fe, Co, Ni, Cu; M^{III} = Cr),[12] formed by three-dimensional chiral oxalate-based networks that behave as ferromagnets, but with critical temperatures that are much lower than those of their 2D counterparts. This has been related to the weaker magnetic interactions present in this case, promoted by a different relative orientation of the magnetic orbitals and to larger metal-to-metal distances. Most of these compounds show T_c below 3 K, with a few exceptions that reach up to 6 K.

The added value of these 3D magnets is their chirality, especially as the crystallites are chiral through self-assembly, even starting from a racemic mixture of building blocks. This family constitutes a nice example of chiral magnets, a very sought after combination in recent years[22–24] because of the interest in the investigation of how chirality affects the magnetic properties: it is easy to understand that the imposed anisotropy in such systems will be a key factor that controls the magnetic behavior, but

[a] Instituto de Ciencia Molecular, Universidad de Valencia, Dr. Moliner 50, 46100 Burjasot, Spain
E-mail: eugenio.coronado@uv.es
jose.r.galan@uv.es
[b] Dept. Química, ITN/CFMC-UL, 2686-953 Sacavém, Portugal

further, that these systems could also exhibit new physical phenomena, for example, the so-called magnetochiral dichroism.[25]

While the dimetallic 2D magnets have been obtained with a variety of trivalent metals, the analogous 3D systems have only been obtained so far for Cr^{III}. The reason is that the synthetic conditions required for the preparation of the 3D systems are much more exigent. For instance, the presence of alkali metals in solution needs to be avoided, since alkali metals can also form 3D networks with trivalent metals with the general formula $[Z^{II}(bpy)_3][A^{I}M^{III}(ox)_3]$ (Z^{II} = Ru, Fe, Co, Ni; A^{I} = Li, Na, K; M^{III} = Cr).[26] These materials have shown interesting electronic properties, such as photoinduced energy transfer, electron transfer,[27] and spin transition in one case, namely $[Co(bpy)_3][LiCr(ox)_3]$,[28,29] but no magnetic ordering since the paramagnetic centers are isolated by diamagnetic alkali neighbors. In addition, more synthetic difficulties need to be overcome, as the trisoxalate complexes are less stable towards ligand substitution. In this work, we present our successful extension of this series to the $[Fe^{III}(ox)_3]^{3-}$ building block while searching for increased ordering temperatures for these magnets, as observed in the 2D analogs.

Results and Discussion

Synthesis and Structure

For the synthesis of the desired $[M^{II}M^{III}(ox)_3]^-$ 3D network, the possible formation of the 3D $[A^{I}M^{III}(ox)_3]^{2-}$ analog, where A^{I} is an alkali metal or a small cation such as NH_4^+, is one of the main synthetic problems to overcome. Thus, the common $A_3[M^{III}(ox)_3]$ salts cannot be used in this synthesis. Bulky cations cannot be used either, since they template the formation of the corresponding 2D honeycomb networks. To form the 3D $[M^{II}Cr^{III}(ox)_3]^-$ network we already described the use of the silver salt $Ag_3[Cr^{III}(ox)_3]$. The same procedure, however, cannot be used to prepare the $M^{II}Fe^{III}$ derivatives since the $Ag_3[Fe(ox)_3]$ salt is unstable. Thus, we used an analogous procedure, but starting from the slightly more soluble $Tl_3[Fe(ox)_3]$ salt that allows for the precipitation of TlCl, and for the preparation of the desired solution containing the M^{II} and $[Fe(ox)_3]^{3-}$ building blocks exclusively. The mixture of this solution with one containing $[Z^{II}(bpy)_3][ClO_4]_2$ yields a fine powder that must be settled before filtering. Particle sizes are typically uniform and of the order 0.5–3 µm.

Even under these conditions not all possible Z/M^{II} combinations that may be suitable for the formation of oxalate complexes could be obtained, as the $[Fe(ox)_3]^{3-}$ complex is not completely stable in solution when competing with other cations. Because of this reason, the nature of the solvent mixture and temperature are crucial to obtain pure products, and even under such circumstances, some disorder between the alternating positions for trivalent and divalent metals in the network cannot be avoided in some cases, as will be discussed in this paper.

All compounds were structurally characterized by powder X-ray diffraction, which indicates that all compounds are isostructural as the salt $[Ru^{II}(bpy)][ClO_4][Mn^{II}Cr^{III}(ox)_3]$ already reported.[12] The structure of these salts consists of 3D oxalate-bridged dimetallic networks that host the cations $[Z^{II}(bpy)_2]^{2+}$ (Figure 1). In the anionic network, the bidentate chelating oxalate ligands connect the metals in an alternating way such that each M^{II} center is surrounded by three M^{III} centers and vice versa, to form 10-unit rings with a (10,3) topology. In a given crystal, all metal centers are of the same chirality, although crystallites of both chiralities are obtained when starting from racemic mixtures of the reagents, as in the compounds prepared for this study. The cations $[Z^{II}(bpy)_3]^{2+}$ of each chiral group template the formation of the corresponding chiral network, and are located in the tunnels left by the polymeric structure. Perchlorate anions fill up the remaining holes in the structure.
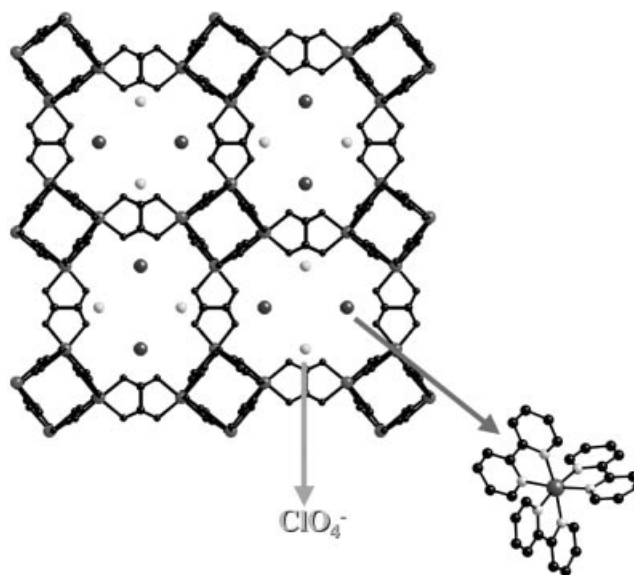

Figure 1. Projection on the *bc* plane of the structure of the family of molecule-based magnets $[Z^{II}(bpy)_3][ClO_4][M^{II}M^{III}(ox)_3]$. Only the Z^{II} ion of the $[Z^{II}(bpy)_3]^{2+}$ cations and the Cl atom of the ClO_4^- anions are drawn in the cavities.

Magnetic Properties

Magnetic susceptibility measurements for the $[Fe^{II}(bpy)_3][ClO_4][M^{II}Fe^{III}(ox)_3]$ derivatives (M^{II} = Mn, Fe) are shown in Figure 2. Both compounds present a clear decrease in the $\chi_m T$ product as the temperature is decreased. This high-temperature regime follows a Curie–Weiss law, and gives Curie constants slightly higher than that expected for spin-only, and large and negative Weiss constants (Table 1), which is indicative of the presence of antiferromagnetic interactions between the metal centers in the network, as is expected for oxalate-bridged dimetallic M^{II}-Fe^{III} compounds. The variation of χ_m with temperature shows a deviation from the regular paramagnetic behavior at low temperatures for both compounds –a jump appears below

E. Coronado, J. R. Galán-Mascarós et al.

Table 1. Magnetic parameters for the series $[Z^{II}(bpy)_3][ClO_4][M^{II}Fe(ox)_3]$.[a]

Z^{II}	M^{II}	T_c [K]	θ [K]	C [emu K mol^{-1}]	$C_{\text{spin-only}}$ [emu K mol^{-1}]	$H_{\text{coer.}}$ [mT]
Fe	Mn	20.0	−58	9.53	8.75	25
Fe	Fe	9.1	−41	7.67	7.375	97
Ru	Mn	17.2	−81	9.46	8.75	30
Ru	Fe	7.9	−46	7.67	7.375	86

[a] T_c, ordering temperature; θ, Weiss constant; C, Curie constant; $H_{\text{coer.}}$, coercive field at 2 K.

25 K for Mn^{II} (Figure 2 bottom) and below 12 K for Fe^{II}. After this jump, χ_m does not tend to saturation at very low temperatures in either compound, showing a Curie tail probably because of the presence of small amounts of paramagnetic impurities. These features suggest the appearance of a magnetically ordered regime. This was confirmed by the temperature dependence of the AC magnetic susceptibility (Figure 3), that shows, in both cases, a maximum in χ'_m that corresponds to a peak in χ''_m, with T_c (when χ''_m becomes non zero) at 20.0 K for the Mn derivative and 9.1 K for the Fe derivative. Due to the nature of the short-range interactions in both cases, the Mn^{II} derivative can be considered to be a weak ferromagnet, and the origin for net magnetization comes from canting between the antiferromagnetically aligned $S(Mn^{II}) = S(Fe^{III}) = 5/2$ moments, while the Fe^{II} derivative can be considered to be a ferrimag-

net, because of the non total compensation of the antiferromagnetically coupled spins $S(Fe^{III}) = 5/2$ and $S(Fe^{II}) = 2$. In this last compound, a small frequency dependence of the AC peaks is observed, similar to those observed in the analogous 2D network. As in these cases, such a feature can be associated to a disorder in the magnetic 3D network generated by partial substitution of the Fe^{II} centers by Fe^{III}, and vice versa. The field dependence of the magnetization at 2 K for both compounds (Figure 4) shows an almost linear increase, and is far from saturation even at 5 T, confirming the nature of the magnetic ordering. Both compounds show small hysteresis loops at 2 K with coercive fields of 25 (Mn^{II}) and 97 mT (Fe^{II}).
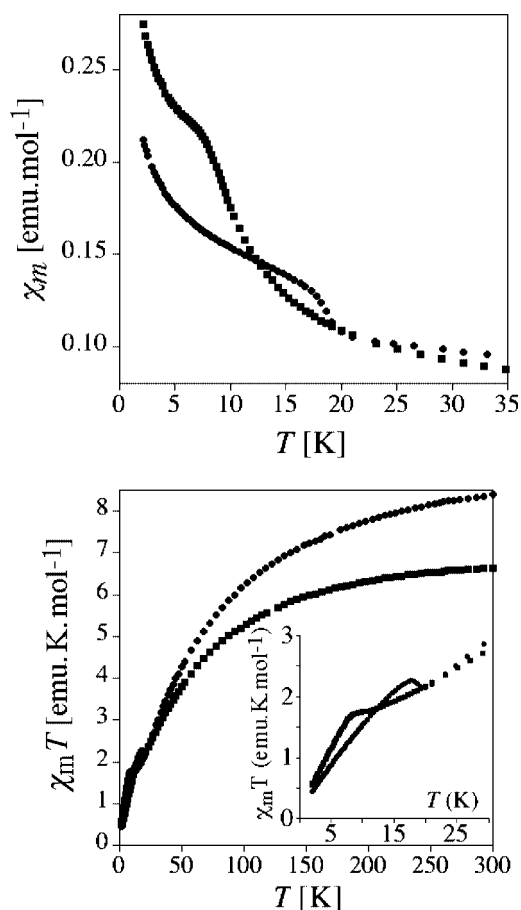

Figure 2. Thermal variation of the magnetic susceptibility χ_m (top) and of the $\chi_m T$ product (bottom) for the salts $[Fe(bpy)_3][ClO_4]$-$[M^{II}Fe(ox)_3]$; M^{II} = Mn (circle), Fe (square).
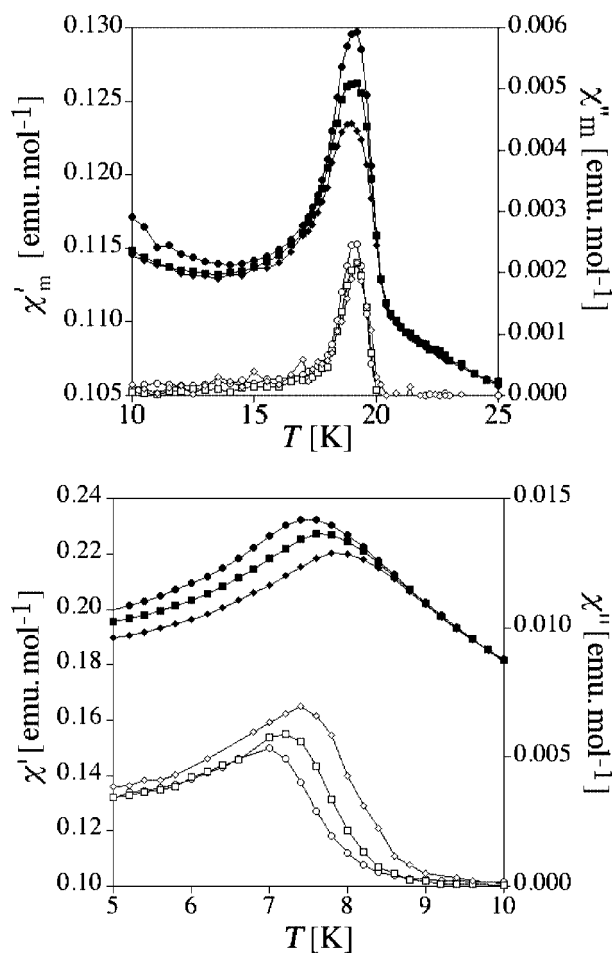

Figure 3. Frequency dependence of the in-phase (filled symbols, χ'_m) and out-of-phase (empty symbols, χ''_m) AC susceptibility of the salts $[Fe(bpy)_3][ClO_4][M^{II}Fe(ox)_3]$ at 1 (circle), 10 (square) and 110 Hz (diamond); M^{II} = Mn (top), Fe (bottom).
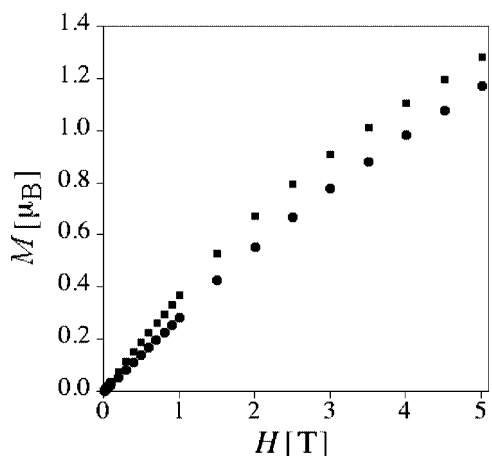
Figure 4. Field dependence of the magnetization at 2 K for the salts $[Fe(bpy)_3][ClO_4][M^{II}Fe(ox)_3]$; M^{II} = Mn (circle), Fe (square).

The $[Ru^{II}(bpy)_3]^{2+}$ derivatives show, as expected, an analogous magnetic behavior, with magnetic parameters very similar to those of the $[Fe^{II}(bpy)_3]^{2+}$ counterparts (see Table 1). The critical temperatures, however, are slightly lower for these derivatives. As mentioned before, this effect
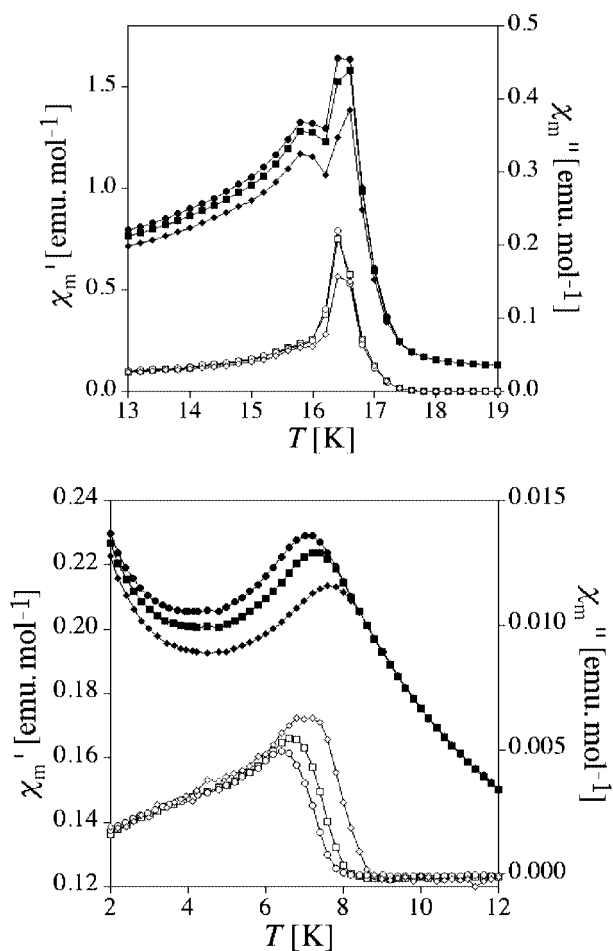

Figure 5. Frequency dependence of the in-phase (filled symbols, χ'_m) and out-of-phase (empty symbols, χ''_m) AC magnetic susceptibility for the salts $[Ru(bpy)_3][ClO_4][M^{II}Fe(ox)_3]$ at 1 (circle), 10 (square) and 332 Hz (diamond); M^{II} = Mn (top), Fe (bottom).

of the templating cation on the magnetic properties was also observed in the Cr^{III} derivatives, and works here in the same direction. The AC magnetic susceptibility measurements (Figure 5) show ordering temperatures at 17.2 K for Mn^{II} and 7.9 K for Fe^{II}. The Mn^{II} salt shows a small maximum in χ'_m after the peak, unseen in the rest of materials. This feature has no frequency dependence and no clear origin. As seen before, the Fe^{II} salt shows a small frequency dependence of the peaks. Both compounds show hysteresis loops below T_c, with coercive fields and field dependence of the magnetization at 2 K, which is almost identical to those of their $[Fe^{II}(bpy)_3]^{2+}$ counterparts. The weaker magnetic exchange when going from $[Fe^{II}(bpy)_3]^{2+}$ to $[Ru^{II}-(bpy)_3]^{2+}$ has been explained in terms of the different size of the cations, which leads to larger unit cells, and therefore larger intermetallic distances; an effect that obviously influences the magnetic properties.

Mössbauer Spectroscopy

Mössbauer spectra of $[Fe(bpy)_3]ClO_4[MnFe(ox)_3]$ were taken at 100 and 6 K (Figure 6). At 100 K, the spectrum consists of three different doublets whose estimated parameters, isomer shift, δ, and quadrupole splitting, Δ, (Table 2), are typical of low-spin (LS) Fe^{II} in a $[Fe(bpy)_3]^{2+}$ complex, of high-spin (HS) Fe^{III} within the anionic oxalate net, and of HS Fe^{II} in the same oxalate net. This HS Fe^{II} is certainly due to impurities in the sample. Incorporation of Fe^{II} into the anionic network was already observed in similar $[Fe(bpy)_3][Mn_2(ox)_3]$ compounds.[32] The spectrum at 6 K (Figure 6) shows a doublet due to LS Fe^{II} in the $[Fe-(bpy)_3]^{2+}$ complex (Table 2), a sextet with broad peaks attributed to HS Fe^{III} and a third set of low-intensity peaks. The HS Fe^{III} contribution is a sextet because the relaxation frequency of the corresponding Fe spins strongly decreases between 100 K and 6 K, and becomes significantly lower than the Larmor period of the nuclear moment. This is a strong indication that the $[MnFe(ox)_3]^-$ net is magnetically ordered at 6 K, which is in agreement with the T_c value deduced from magnetization data. It should be noted that LS Fe^{II} in the $[Fe(bpy)_3]^{2+}$ complex remains unaffected by the internal magnetic field.
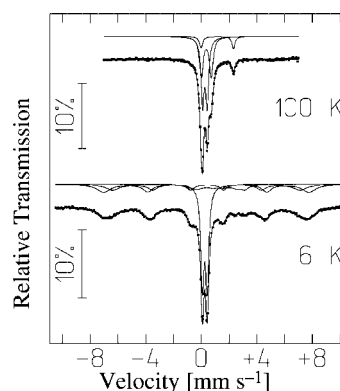

Figure 6. Mössbauer spectra at different temperatures for the salt $[Fe(bpy)_3][ClO_4][MnFe(ox)_3]$.

Table 2. Estimated parameters from the Mössbauer spectra of $[Fe(bpy)_3][ClO_4][MnFe(ox)_3]$ at different temperatures.[a]

T [K]	Fe site	δ [mm s^{-1}]	Δ, Δ', ε [mm s^{-1}]	B_{hf} [T]	η	Θ [°]	Φ	%
100	$[Fe(bpy)_3]^{2+}$	0.37	0.33	–	–	–	–	51
	$[Fe^{III}(ox)_{3/2}]$	0.46	0.72	–	–	–	–	40
	$[Fe^{II}(ox)_{3/2}]^-$	1.26	2.33	–	–	–	–	9
6	$[Fe(bpy)_3]^{2+}$	0.37	0.35	–	–	–	–	41
	$[Fe^{III}(ox)_{3/2}](1)$	0.50	−0.06	47.6	–	–	–	31
	$[Fe^{III}(ox)_{3/2}](2)$	0.50	0.01	41.6	–	–	–	17
	$[Fe^{II}(ox)_{3/2}]^-$	1.29	−1.69	8.5	1	90	0	11

[a] δ, isomer shift relative to metallic α-Fe at 295 K; Δ, quadrupole splitting in the paramagnetic state; Δ' and ε, quadrupole interaction and quadrupole shift in the magnetically ordered state for Fe^{II} and Fe^{III}, respectively; B_{hf}, magnetic hyperfine field; η, asymmetry parameter; Θ and Φ, angles between B_{hf} and the main axis V_{zz} of the electric field gradient and between B_{hf} and the main axis V_{xx}; %, percentage of the total area corresponding to each subunit. Estimated errors are ≤ 0.02 mm s^{-1} for δ, Δ, Δ' and <0.2 T for B_{hf}. Values of Θ, Φ and η, kept constant during the fitting procedure, are those corresponding to the best final adjustments.

Considering the 100 K spectrum, the third set of low-intensity peaks observed at 6 K is most likely due to the HS Fe^{II} impurities in the oxalate net. These Fe^{II} atoms are also magnetically ordered. However, as previously shown,[14] their contribution cannot be fitted assuming a simple magnetic sextet. In fact, the quadrupole hyperfine interaction cannot be treated as a perturbation of the magnetic hyperfine interaction. The position and relative intensities of the absorption lines of the magnetically ordered HS Fe^{II} atoms therefore have to be calculated by solving the complete Hamiltonian for the hyperfine interactions in both the excited and ground nuclear states of the ^{57}Fe nuclei. In the present work, this calculation was performed following the procedure described by Ruebenbauer and Birchall.[30] The best fit was obtained assuming that the angle between B_{hf} and the main axis of the electric field gradient, V_{zz}, is $\Theta = 90$, and between V_{xx} and B_{hf} is $\Phi = 0$. The final values obtained for the fitted parameters, δ, B_{hf}, the asymmetry parameter η, and $\Delta' = e^2QV_{zz}$ (where e is the electron charge and Q is the ^{57}Fe nuclear quadrupole moment at the 14.4 keV level), are given in Table 2. The estimated parameters obtained are indeed consistent with a HS Fe^{II} atom and similar to those reported for compounds containing $[Fe^{II}(ox)_{3/2}]^-$ units.[14,31] The random substitution of Mn^{II} by these Fe^{II} impurities within the oxalate network gives rise to different environments for the HS Fe^{III} atoms. Differences in the magnetic exchange interactions, which correspond to distinct environments, may be large enough to be observed as a distribution of B_{hf}. This distribution, approximately described by two sextets, whose parameters are summarized in Table 2, explains the broadness of the observed peaks due to the HS Fe^{III} atoms in the oxalate layers and the small frequency dependence of the χ'' peak observed in the AC susceptibility data.

The relative areas estimated for LS Fe^{II} and HS Fe^{III} change significantly between 100 K and 6 K. This fact had already been observed in $[Fe(bpy)_3][M^{II}_2(ox)_3]$ (M = Mn, Fe) compounds that also contained HS Fe^{II} impurities.[32] It may be explained by the different temperature dependence of the Debye–Waller factors for LS Fe^{II} and HS Fe^{III}. Considering that the values of these factors are closer at the lowest temperatures, the relative areas estimated at 6 K are

a better approximation to the relative amounts of the different Fe species in the sample. This implies that the HS Fe^{II} impurities that substitute Mn^{II} in the oxalate layers are approximately 10% of the total Fe in the present $[Fe(bpy)_3][ClO_4][MnFe(ox)_3]$ sample; a value similar to those reported for the $[Fe(bpy)_3][M^{II}_2(ox)_3]$ salts.[32]

The Mössbauer spectra of $[Fe(bpy)_3][ClO_4][FeFe(ox)_3]$ at 294 K and 100 K (Figure 7) consist of three doublets attributed to LS Fe^{II} in $[Fe(bpy)_3]^{2+}$, HS Fe^{III} and HS Fe^{II} in the inorganic network (see estimated parameters for $[Fe(bpy)_3]$-$[ClO_4][FeFe(ox)_3]$ and $[Fe(bpy)_3][ClO_4][MnFe(ox)_3]$ in Table 2 and Table 3). At 6 K, the spectrum shows that the HS Fe^{III} and HS Fe^{II} atoms in the inorganic network have a slow relaxation, which is consistent with the magnetic ordering of these Fe species and in agreement with the magnetic data. As in the case of $[Fe(bpy)_3][ClO_4[MnFe(ox)_3]$, LS Fe^{II} in $[Fe(bpy)_3]^{2+}$ remains unaffected by the internal
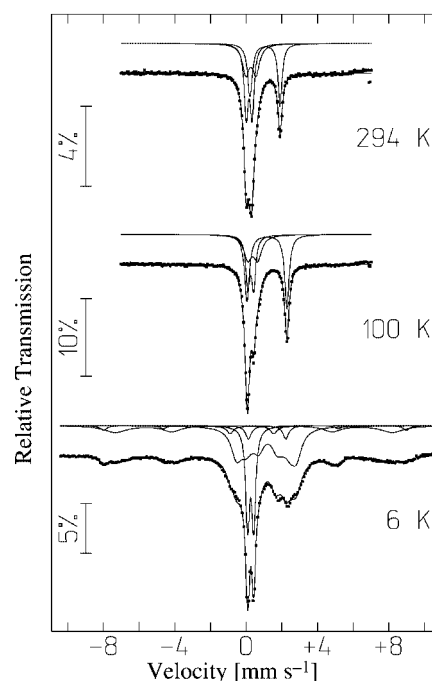

Figure 7. Mössbauer spectra at different temperatures for the salt $[Fe(bpy)_3][ClO_4][FeFe(ox)_3]$.

Table 3. Estimated parameters from the Mössbauer spectra of $[Fe(bpy)_3][ClO_4][FeFe(ox)_3]$ at different temperatures.[a]

T [K]	Fe site	δ [mm s^{-1}]	Δ, Δ', ε [mm s^{-1}]	B_{hf} [T]	η	Θ [°]	Φ	%
294	$[Fe(bpy)_3]^{2+}$	0.28	0.33	–	–	–	–	38
	$[Fe^{III}(ox)_{3/2}]$	0.38	0.57	–	–	–	–	28
	$[Fe^{II}(ox)_{3/2}]^-$	1.17	1.69	–	–	–	–	34
100	$[Fe(bpy)_3]^{2+}$	0.37	0.33	–	–	–	–	28
	$[Fe^{III}(ox)_{3/2}]$	0.45	0.57	–	–	–	–	26
	$[Fe^{II}(ox)_{3/2}]^-$	1.28	2.24	–	–	–	–	46
6	$[Fe(bpy)_3]^{2+}$	0.37	0.34	–	–	–	–	25
	$[Fe^{III}(ox)_{3/2}](1)$	0.49	0.11	48.1	–	–	–	20
	$[Fe^{III}(ox)_{3/2}](2)$	0.49	0.23	52.6	–	–	–	4
	$[Fe^{II}(ox)_{3/2}]^-(1)$	1.29	1.84	6.2	0.8	90	0	46
	$[Fe^{II}(ox)_{3/2}]^-(2)$	1.29	2.10	–	–	–	–	5

[a] Parameters as defined in Table 2.

magnetic field. The relative areas estimated for HS Fe^{III} and Fe^{II} at 6 K suggest that in $[Fe(bpy)_3][ClO_4][FeFe(ox)_3]$, there is an excess of HS Fe^{II} that could replace HS Fe^{III} in random positions in the oxalate layer. This disorder may be responsible for the observation of a distribution of B_{hf} for HS Fe^{III}, again approximated by two magnetic sextets with large peak widths, as in $[Fe(bpy)_3][ClO_4][MnFe(ox)_3]$. Furthermore, the same disorder may explain why acceptable fits of the 6 K spectrum could only be obtained if a doublet corresponding to paramagnetic HS Fe^{II} was considered in addition to the main magnetically ordered contribution of this Fe species (Table 3). In fact, the disorder resulting from the presence of excess HS Fe^{II} may be associated with the existence of small fractions of these ions that experience rapidly fluctuating B_{hf} even at temperatures lower than T_c (although still close to T_c).

Conclusions

In this paper we have demonstrated that 3D chiral molecular magnets based on dimetallic oxalate complexes can be prepared from the $[Fe(ox)_3]^{3-}$ building block given the right synthetic conditions and with the use of different $[Z^{II}(bpy)_3]^{2+}$ complexes (Z^{II} = Fe, Ru) as templating cations. The salts $[Z^{II}(bpy)_3][ClO_4][M^{II}Fe^{III}(ox)_3]$ (M^{II} = Mn, Fe) are isostructural to the $[Cr(ox)_3]^{3-}$-based ferromagnets and are of identical stoichiometry, while the different sign and strength of the magnetic exchange promoted by the presence of Fe^{III} instead of Cr^{III} yields quite different magnetic properties. As these compounds exhibit strong antiferromagnetic interactions, they behave as ferrimagnets (M^{II} = Fe) or weak ferromagnets (M^{II} = Mn) with critical temperatures in the range 7–20 K, which are much higher than those observed for the analogous ferromagnets, in which the ordering only occurred close to 2 K. This fact must be important in the future studies that investigate the interplay between magnetism and chirality.

Another consideration that needs to be stressed is the effect of the nature of the $[Z^{II}(bpy)_3]$ complex on the magnetic properties. With the same crystal structure, the different sizes of the cations promote an enlargement of the

unit cell parameters by 0.2 Å. Such small differences are enough to provoke a change of a few degrees in T_c, as seen in this and other cases. This suggests that hydrostatic pressure should also be able to affect the magnetic properties in these materials. Thus, magnetic measurements under pressure are in progress.

Experimental Section

Synthesis: The complexes $[Z^{II}(bpy)_3]^{2+}$ (Z^{II} = Ru, Fe) were prepared according to literature methods.[33,34] The precursor salt $Tl_3[Fe(ox)_3]\cdot nH_2O$ was prepared by metathesis from the corresponding potassium salt.[35] All other materials and solvents were commercially available and used without further purification.

$[Z^{II}(bpy)_3][ClO_4][M^{II}Fe^{III}(ox)_3]$ (Z^{II} = Fe, Ru; M^{II} = Mn, Fe): $M^{II}Cl_2$ (1.56 mmol) was added in excess to a water solution (10 mL) of $Tl_3[Fe(ox)_3]\cdot nH_2O$ (0.3 g, 0.31 mmol). After stirring for 10 min, a white precipitate of TlCl was removed by filtration. DMF (20 mL) was added to this green solution, which then turned yellow, and this mixture was added dropwise to a DMF (15 mL) solution of $[Z^{II}(bpy)_3][ClO_4]_2$ (0.4 mmol). After stirring for 30 min, the mixture was cooled down to 5 ºC overnight. The product was isolated by filtration with use of a vacuum, washed thoroughly with methanol and acetone, and dried at room temperature.

FeMnFe: Yield 61% (183 mg). $C_{36}H_{24}ClFe_2MnN_6O_{16}$ (998.70): calcd. C 43.30, H 2.42, N 8.42; found C 43.18, H 2.30, N 8.35.

FeFeFe: Yield 55% (165 mg). $C_{36}H_{24}ClFe_3N_6O_{16}$ (999.61): calcd. C 43.36, H 2.42, N 8.41; found C 42.95, H 2.11, N 8.10.

RuMnFe: Yield 75% (235 mg). $C_{36}H_{24}ClFeMnN_6O_{16}Ru$ (1043.92): calcd. C 41.42, H 2.32, N, 8.05; found C 41.20, H 2.22, N 7.99.

RuFeFe: Yield 80% (251 mg). $C_{36}H_{24}ClFe_2N_6O_{16}Ru$ (1044.87): calcd. C 41.38, H 2.32, N 8.04; found C 40.93, H 2.12, N 7.80.

Structural Characterization: X-ray powder profiles were collected with a Siemens D-500 X-ray diffractometer (Cu-K_a radiation, λ_a = 1.54184 Å) at 293(2) K. Samples were grounded and mounted on a flat sample plate. Typically, profiles were collected as step scans over a 12 h period in the $2 < 2\theta < 60$ range with a step size of 0.02. The powder diffraction profiles indicate that all compounds are isostructural and show analogous patterns to the simulated profile[36] from the atomic positional parameters of the published crystal structure of $[Ru(bpy)_3][ClO_4][MnCr(ox)_3]$,[12] which has the cubic space group $P4_132$ (see Supporting Information). Indexation

of the main reflections[37] gave the unit cell parameters shown in Table 4.

Table 4. Crystallographic data for the salts [Z^{II}(bpy)$_3$][ClO$_4$]-[$M^{II}M^{III}$(ox)$_3$].

$Z^{II}M^{II}M^{III}$	a [Å]	V [Å^3]
FeMnFe	15.39(3)	3645(1)
FeFeFe	15.33(2)	3603(1)
RuMnFe	15.48(4)	3709(1)
RuFeFe	15.44(4)	3681(1)

Magnetic Measurements: Magnetic susceptibility measurements were performed on polycrystalline samples with a Quantum Design MPMS-XL-5 susceptometer equipped with a SQUID sensor. The susceptibility data were corrected from the diamagnetic contributions as deduced by using Pascal's constant tables. DC data were collected in the range 2–300 K with an applied field of 0.1 T, and hysteresis loops were collected between –5 and +5 T at 2 K. AC data were collected in the range 2–30 K with an applied alternating field of 0.395 mT at different frequencies in the range 1–997 Hz.

Mössbauer Spectroscopy: ^{57}Fe Mössbauer measurements were recorded in transmission mode with a conventional constant acceleration spectrometer and a 25-mCi ^{57}Co source in Rh matrix. The velocity scale was calibrated by using an α-Fe foil at room temperature. Isomer shift values are given relative to this standard. Spectra were collected with the absorbers between 296 K and 5 K. Low-temperature measurements were obtained with a flow cryostat (temperature stability 0.5 K). The spectra were fitted to Lorentzian lines by using a non-linear least-squares fitting method as described previously.[38]

Acknowledgments

[1] K. R. Dunbar, R. A. Heintz, *Prog. Inorg. Chem.* **1997**, *45*, 283–391.

[2] M. Kurmoo, C. J. Kepert, *New J. Chem.* **1998**, *22*, 1515–1524.

[3] J. L. Manson, C. R. Kmety, Q. Z. Huang, J. W. Lynn, G. M. Bendele, S. Pagola, P. W. Stephens, L. M. Liable-Sands, A. L. Rheingold, A. J. Epstein, J. S. Miller, *Chem. Mater.* **1998**, *10*, 2552–2560.

[4] a) S. R. Batten, K. S. Murray, *Coord. Chem. Rev.* **2003**, *246*, 103–130; b) S. R. Batten, P. Jensen, B. Moubaraki, K. S. Murray, R. Robson, *Chem. Commun.* **1998**, 430–440.

[5] H. Tamaki, Z. J. Zhong, N. Matsumoto, S. Kida, M. Koikawa, N. Achiwan, Y. Hashimoto, H. Okawa, *J. Am. Chem. Soc.* **1992**, *114*, 6974–6979.

[6] C. Mathonière, C. J. Nuttall, S. G. Carling, P. Day, *Inorg. Chem.* **1996**, *35*, 1201–1206.

[7] R. Pellaux, H. W. Schamalle, R. Hubert, P. Fisher, T. Hauss, B. Ouladiaff, S. Decurtins, *Inorg. Chem.* **1997**, *36*, 2301–2308.

[8] J. R. Galán-Mascarós, K. R. Dunbar, *Angew. Chem. Int. Ed.* **2003**, *42*, 2289–2293.

[9] E. Coronado, J. R. Galán-Mascarós, C. J. Gómez-García, *J. Chem. Soc. Dalton Trans.* **2000**, 205–210.

[10] E. Coronado, J. R. Galán-Mascarós, C. Giménez-Saiz, C. J. Gómez-García, C. Ruíz-Pérez, *Eur. J. Inorg. Chem.* **2003**, 2290–2298.

[11] E. Coronado, J. R. Galán-Mascarós, C. Martí-Gastaldo, manuscript in preparation.

[12] E. Coronado, J. R. Galán-Mascarós, C. J. Gómez-García, J. M. Martínez-Agudo, *Inorg. Chem.* **2001**, *40*, 113–120.

[13] S. Decurtins, H. W. Schmalle, P. Schneuwly, J. Enslin, P. Gütlich, *J. Am. Chem. Soc.* **1994**, *116*, 9521–9528.

[14] E. Coronado, J. R. Galán-Mascarós, C. J. Gómez-García, J. M. Martínez-Agudo, E. Martínez-Ferrero, J. C. Waerenborgh, M. Almeida, *J. Solid State Chem.* **2001**, *159*, 391–402.

[15] J. Larionova, B. Mombelli, J. Sanchiz, O. Kahn, *Inorg. Chem.* **1998**, *37*, 679–684.

[16] E. Coronado, J. R. Galán-Mascarós, C. J. Gómez-García, E. Martínez-Ferrero, S. van Smaalen, *Inorg. Chem.* **2004**, *43*, 4808–4810.

[17] E. Coronado, J. R. Galán-Mascarós, C. J. Gómez-García, J. M. Martínez-Agudo, *Adv. Mater.* **1999**, 558–561.

[18] E. Coronado, J. R. Galán-Mascarós, C. J. Gómez-García, J. Ensling, P. Gütlich, *Chem. Eur. J.* **2000**, *6*, 552–563.

[19] E. Coronado, J. R. Galán-Mascarós, C. J. Gómez-García, V. Laukhin, *Nature* **2000**, *408*, 447–449.

[20] A. Alberola, E. Coronado, J. R. Galán-Mascarós, C. Giménez-Saiz, C. J. Gómez-García, *J. Am. Chem. Soc.* **2003**, *125*, 10774–10775.

[21] S. Bénard, P. Yu, J. P. Audière, E. Rivière, R. Clément, J. Guilhem, L. Tchertanov, K. Nakatani, *J. Am. Chem. Soc.* **2000**, *122*, 9444–9454.

[22] K. Inoue, H, Imai, P. S. Ghalsasi, K. Kikuchi, M. Ohba, H. Okawa, J. V. Yakhmi, *Angew. Chem. Int. Ed.* **2001**, *40*, 4242–4245.

[23] E.-Q. Gao, Y.-F. Yue, S.-Q. Bai, Z. He, C.-H. Yan, *J. Am. Chem. Soc.* **2004**, *126*, 1419–1429.

[24] R. Feyerherm, A. Loose, T. Ishida, T. Nogami, J. Kreitlow, D. Baabe, F. J. Litterst, S. Süllow, H.-H. Klauss, K. Doll, *Phys. Rev. B* **2004**, *69*, 134427.

[25] G. L. J. A. Rikken, E. Raupach, *Nature* **1997**, *390*, 493–494.

[26] S. Decurtins, H. W. Schmalle, P. Schneuwly, H. R. Oswald, *Inorg. Chem.* **1993**, *32*, 1888–1892.

[27] S. Decurtins, H. W. Schmalle, R. Pellaux, P. Schneuwly, A. Hauser, *Inorg. Chem.* **1996**, *35*, 1451–1460.

[28] A. Hauser, H. Riesen, R. Pellaux, S. Decurtins, *Chem. Phys. Lett.* **1996**, *261*, 313–317.

[29] R. Sieber, S. Decurtins, H. Stoeckli-Evans, C. Wilson, D. Yufit, J. A. K. Howard, S. C. Capelli, Hauser, A. *Chem. Eur. J.* **2000**, *6*, 361–368.

[30] K. Ruebenbauer, T. Birchall, *Hyper. Interact.* **1979**, *7*, 125–133.

[31] S. G. Carling, D. Visser, D. Hautot, I. D. Watts, P. Day, J. Ensling, P. Gütlich, G. J. Long, F. Grandjean, *Phys. Rev. B.* **2002**, *66*, 104407–104419.

[32] S. Decurtins, H. W. Schmalle, P. Schneuwly, J. Ensling, P. Gütlich, *J. Am. Chem. Soc.* **1994**, *116*, 9521–9528.

[33] F. H. Burstall, R. S. Nyholm, *J. Chem. Soc.* **1952**, 3570–3579.

[34] S. Anderson, K. R. Seddon, *J. Chem. Res.* **1979**, 75–77.

[35] J. M. Baylar, E. M. Jones, in *Inorganic Synthesis* (Ed.: H. S. Booth), McGraw-Hill, Nueva York, **1939**, vol. 1, p. 35.

[36] *CrystalDiffract 4.0.2* (CrystalMaker software).

[37] *CELSIZ* (Unit Cell Refinement v1.1 XRDUtilities).

[38] J. C. Waerenborgh, M. O. Figueiredo, J. M. P. Cabral, L. C. J. Pereira, *Phys. Chem. Miner.* **1994**, *21*, 460–468.